ARL

US Army Research Laboratory

Shack-Hartmann Electron Densitometer (SHED): An Optical System for Diagnosing Free Electron Density in Laser-Produced Plasmas

by Anthony R Valenzuela

NOTICES

Disclaimers

US Army Research Laboratory

Shack-Hartmann Electron Densitometer (SHED): An Optical System for Diagnosing Free Electron Density in Laser-Produced Plasmas

by Anthony R Valenzuela
Weapons and Materials Research Directorate, ARL

REPORT DOCUMENTATION PAGE				*Form Approved* *OMB No. 0704-0188*
Public reporting burden for this collection of information is estimated to average 1 hour per response, including the time for reviewing instructions, searching existing data sources, gathering and maintaining the data needed, and completing and reviewing the collection information. Send comments regarding this burden estimate or any other aspect of this collection of information, including suggestions for reducing the burden, to Department of Defense, Washington Headquarters Services, Directorate for Information Operations and Reports (0704-0188), 1215 Jefferson Davis Highway, Suite 1204, Arlington, VA 22202-4302. Respondents should be aware that notwithstanding any other provision of law, no person shall be subject to any penalty for failing to comply with a collection of information if it does not display a currently valid OMB control number. **PLEASE DO NOT RETURN YOUR FORM TO THE ABOVE ADDRESS.**				

1. REPORT DATE *(DD-MM-YYYY)*	2. REPORT TYPE	3. DATES COVERED (From - To)		
November 2016	Technical Report	7 January 2013–30 April 2014		

4. TITLE AND SUBTITLE	5a. CONTRACT NUMBER
Shack-Hartmann Electron Densitometer (SHED): An Optical System for Diagnosing Free Electron Density in Laser-Produced Plasmas	
	5b. GRANT NUMBER
	5c. PROGRAM ELEMENT NUMBER
6. AUTHOR(S)	**5d. PROJECT NUMBER**
Anthony R Valenzuela	
	5e. TASK NUMBER
	5f. WORK UNIT NUMBER

7. PERFORMING ORGANIZATION NAME(S) AND ADDRESS(ES)	8. PERFORMING ORGANIZATION REPORT NUMBER
US Army Research Laboratory ATTN: RDRL-WMP-A Aberdeen Proving Ground, MD 21005-5069	ARL-TR-7868

9. SPONSORING/MONITORING AGENCY NAME(S) AND ADDRESS(ES)	10. SPONSOR/MONITOR'S ACRONYM(S)
	11. SPONSOR/MONITOR'S REPORT NUMBER(S)

12. DISTRIBUTION/AVAILABILITY STATEMENT
Approved for public release; distribution is unlimited.

13. SUPPLEMENTARY NOTES

14. ABSTRACT

The Shack-Hartmann Electron Densitometer is a novel method to diagnose ultrashort pulse laser–produced plasmas by measuring the phase change to a probe laser beam. Free electrons in a plasma cause distortions to the phasefront of a probe laser that is measured through a lenslet array onto a camera. This method allows for superior performance in measuring minute variations in the electron density in 2 dimensions with subpicosecond time resolution. The data taken demonstrated the ability to diagnose plasmas with densities of the order of 10^{19} cm^{-3} and show the temporal evolution of the plasma long after the driving laser pulse has left. The method can be further improved by enclosing the probe beam and adding a second axis to allow for tomographic reconstruction of the electron density in 3 dimensions.

15. SUBJECT TERMS					
plasmas, nonlinear optics, ultrashort pulse lasers, filamentation, plasma diagnostics					

16. SECURITY CLASSIFICATION OF:			17. LIMITATION OF ABSTRACT	18. NUMBER OF PAGES	19a. NAME OF RESPONSIBLE PERSON
					Anthony R Valenzuela
a. REPORT	b. ABSTRACT	c. THIS PAGE	UU	26	19b. TELEPHONE NUMBER (Include area code)
Unclassified	Unclassified	Unclassified			410-278-9876

Standard Form 298 (Rev. 8/98)
Prescribed by ANSI Std. Z39.18

Contents

List of Figures

## Acknowledgments

INTENTIONALLY LEFT BLANK.

1. Introduction

Plasma, an ionized gas, is most often encountered in the form of astronomical-sized bodies known as stars, familiarly our sun. However, the advent of ultrashort pulse lasers (USPLs) has allowed for the creation of intense plasma sources in the nanoscale of both time and space. USPLs have pulse durations of a few picoseconds or shorter that translate a small amount of energy (tens of joules or less) into enormous peak powers on the order of gigawatts to petawatts. When focused in air, these intense pulses are able to ionize nitrogen and oxygen molecules, creating localized plasma sources. These plasmas diminish as the ionized molecules and atoms recombine with liberated electrons, typically on the timescale of a few nanoseconds. The challenge remains to diagnose plasmas via the free electron density in this short window of time and often in a small volume of space.

USPLs of sufficient intensity are able to augment the index of refraction of transparent media, particularly air. This positive change to the index of refraction causes what is known as Kerr self-focusing. As the intensity increases through focusing, eventually the threshold for ionization is exceeded, creating a plasma as described previously. Plasma itself has the effect of lessening the index of refraction—in fact, the index of refraction is less than one and defocusing occurs. If the self-focusing can be balanced against the defocusing, a quasi-stable propagation state can be achieved known as a filament.[1–3] The filament contains 3 key components: 1) an intense laser core sufficient to create a plasma, 2) an energy reservoir around the core of laser light sufficient to self-focus but less than that required for ionization, and 3) a plasma created by the intense core that lasts a few nanoseconds after the laser pulse. Much insight into filamentation remains to be gained by understanding the plasma and how it evolves in space and time. In particular, research concepts that seek to use the plasma component of filamentation to guide electromagnetic radiation[4–9] and electrical discharges[10–12] would depend critically on the evolution and structure of the free electron density.

Current concepts to measure the free electron density in USPL-created plasmas are limited in the number of space-time dimensions that can be measured simultaneously. One method to measure USPL-created plasmas is to "pick off" a small portion of the laser energy to use as a probe. This allows researchers to probe with subpicosecond time resolution and synchronize with the driving pump pulse. However, the fidelity required to measure small changes in the electron density can be hard to achieve given typical USPL wavelengths, the most common being 800 nm. A common method to do this is to measure the perturbation of the phase of the probe beam when it is interfered against a reference beam, known as

interferometry.[13,14] This method is often limited in sampling only one spatial dimension at a time, and the minimum resolution in phase is related to the probe wavelength. Other methods include measuring the charge generated by the free electrons,[15] holography,[16] or fluorescence.[17,18] However, these methods provide neither great temporal nor spatial resolution simultaneously.

An improved method would enable researchers to gain high 2-D spatial resolution data on the electron density from a single laser pulse. To meet this requirement, the method proposed here incorporates the principle of phase perturbation from interferometry but resolves that through geometrical focusing. This concept is known as Shack-Hartmann interferometry[19] and is derived from a clear need in astronomy to diagnose phase changes to light observed from outer space traveling through terrestrial atmosphere via adaptive optics. In the case discussed here, the phase changes are created by the free electrons accumulated in the phase of the probe laser beam.[20] Shack-Hartmann uses a microlens array to divulge the change to the phasefront of the probe beam as illustrated in Fig. 1. When an unperturbed (reference) beam passes through a microlens array, each lens focuses its portion of the probe beam onto a specific point on a detection device, usually a charge-coupled device (CCD) camera. When the perturbed beam then passes through the microlens array, small changes in the phase cause the focal point to shift on the camera plane. By using complex algorithms, the shift in focal point, Δx_n, can be translated into the change in phase for the sampled section of the probe beam. If we assume a radial symmetric electron density profile (from a radial symmetric laser pulse), we can then infer the electron density variation from the accumulated phase change from that section of the probe beam. From this we can build a rough idea of the electron density variation in the filament. Described in this report is an optical system built around this concept known as the Shack-Hartmann Electron Densitometer (SHED).
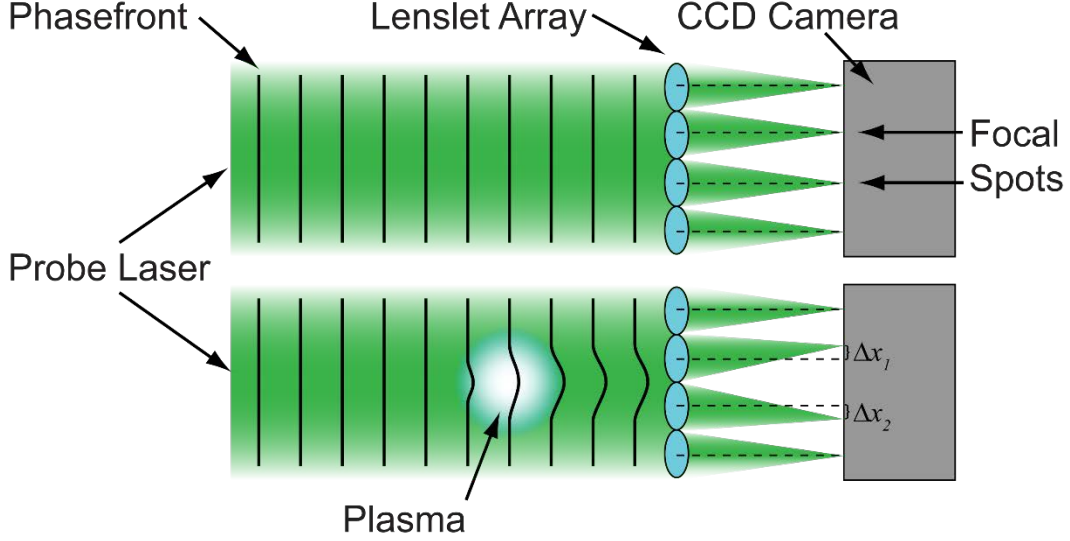
Fig. 1 Shack-Hartmann effect where (top) a probe laser with a known phasefront passes through a lenslet array onto a CCD camera and (bottom) a plasma in the probe path causes changes to the phasefront resulting in displacement, Δxn, of focal spots

2.   Optical Effects of Plasma

Electromagnetic radiation, particularly lasers pulses, is affected by the free electrons in a plasma in a very different manner than other forms of matter. While solids, liquids, and gasses have a refractive index greater than 1 and vacuum has an index of refraction of 1, plasmas have a refractive index between 0 and 1. Because of the comparative mass between electrons and ions, the effects from ions are generally ignored. If we propagate a laser beam with wavelength λ in the **x** direction through a plasma with electron density n_e (Fig. 2a), via Snell's law, we can calculate the change to the phase of the probe, θ, by[20]

$$\theta = \frac{1}{2} \int \frac{\nabla n_e \cdot d\mathbf{x}}{n_{cr}(\lambda)} , \qquad (1)$$

where n_{cr} is the critical density. The equation for the critical density is given as

$$n_{cr}(\lambda) = \epsilon_0 m_e \left(\frac{2\pi c}{\lambda e}\right)^2 \approx \frac{1.12 \times 10^{21}}{\lambda[\mu m]^2} [cm^{-3}] , \qquad (2)$$

where ϵ_0 is the vacuum permittivity, c is the speed of light, and m_e and e are the electron mass and charge, respectively. We will assume 2 different types of plasma geometry: 1) cylindrical from a collimated, radially symmetric plasma and 2) spherical from a plasma that is formed around a specific point and expands with radial symmetry.
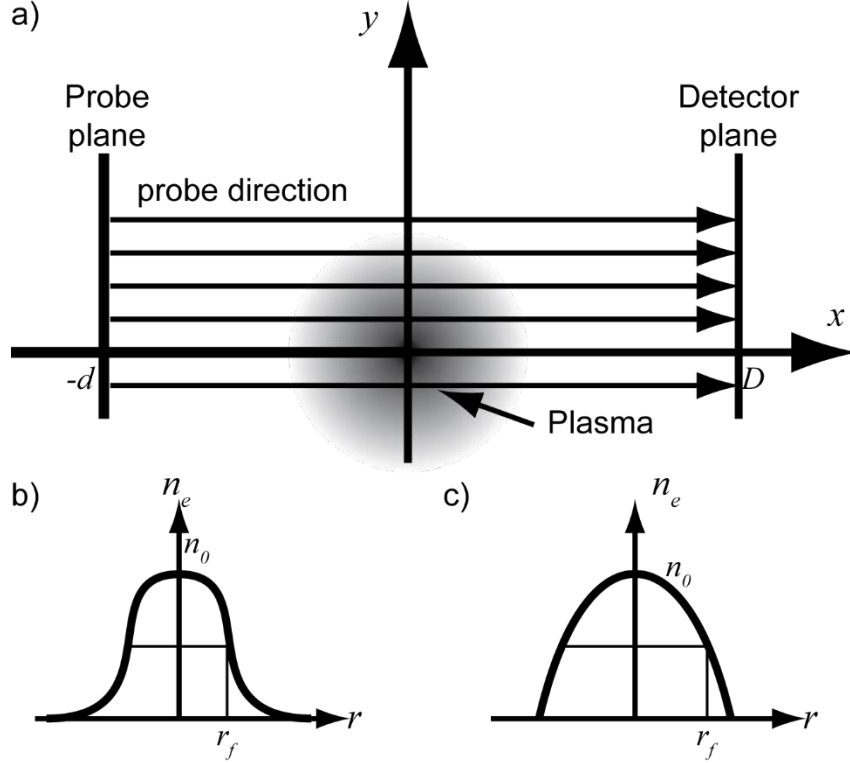
Fig. 2   Illustrations of probe interrogation of plasma a) probe propagates from probe plane to detector plane, b) Gaussian electron density profile, and c) parabolic density profile

2.1 Cylindrical Geometry

This geometry is a first-order approximation of that created in the filamentation process. Let us assume that the cylindrical plasma is along the **z** direction with radial geometry propagating outward in the **x** and **y** directions. We start by breaking the laser probe pulse traveling the in the **x** direction into y components leading to the density gradient of

$$\nabla n_e = \frac{\partial n_e}{\partial y}. \tag{3}$$

If we center the plasma at $x = 0$ and have the probe travel a distance d to the plasma center then a distance D to the detector plane with an optical magnification of M, we can rewrite Eq. 1 given Eq. 3 as

$$\theta_{cyl}(y) = \frac{M}{2n_{cr}} \int_{-d}^{D} \frac{\partial n_e}{\partial y} dx. \tag{4}$$

If we assume a radial Gaussian electron density centered on the z axis (Fig. 2b), then

$$n_{e,G}(r) = n_0 \exp(\alpha r^2), \tag{5}$$

where n_0 is the peak electron density, r is the radius given by $r = \sqrt{x^2 + y^2}$, and

$$\alpha = -\frac{\ln 2}{r_f^2}$$

with r_f being the half-width at half maximum of the extent of the plasma. Substituting into Eq. 4, we arrive at the following equation for integration:

$$\theta_{cyl,G}(y) = \alpha M y \frac{n_0}{n_{cr}} \exp(\alpha y^2) \int_{-d}^{D} \exp(\alpha x^2) dx . \tag{6}$$

Equation 6 can be integrated directly to the solution

$$\theta_{cyl,G}(y) = A_{cyl} y \exp(B_{cyl} y^2) , \tag{7}$$

where

$$A_{cyl} = \gamma \frac{M n_0 \sqrt{\pi}}{2 n_{cr}} [\mathrm{erf}(\gamma D) + \mathrm{erf}(\gamma d)]$$
$$B_{cyl} = -\gamma^2 \qquad .$$
$$\gamma = \sqrt{-\alpha}$$

If instead we assume a parabolic electron density (Fig. 2c) such that

$$n_{e,P}(r) = \begin{cases} n_0 \left(1 - \frac{r^2}{2r_f^2}\right), & r \le \sqrt{2} r_f \\ 0, & r > \sqrt{2} r_f \end{cases} , \tag{8}$$

where we assume $d, D \ge \sqrt{2} r_f$, we then arrive at the following evaluation of Eq. 4:

$$\theta_{cyl,P}(y) = -\frac{M n_0}{2 n_{cr} r_f^2} \int_{-x_0}^{x_0} dx , \tag{9}$$

where $x_0 = \sqrt{2 r_f^2 - y^2}$. Upon integration of Eq. 9, we arrive at

$$\theta_{cyl,P}(y) = -\frac{n_0}{n_{cr}} \frac{M y}{r_f} \sqrt{2 - \left(\frac{y}{r_f}\right)^2}. \tag{10}$$

2.2 Spherical Geometry

Spherical geometry better approximates the plasma created by a sharply focused laser pulse. The mathematics is similar except that we now have plasma density variation in the z direction, too. We again assume radially symmetric density variations that lead to a revision of Eq. 3 to be

$$\nabla n_e = \frac{\partial}{\partial \rho} n_e(r) \, , \tag{11}$$

where

$$\rho^2 = y^2 + z^2$$
$$r^2 = \rho^2 + x^2 \cdot$$

This leads to a new equation for the deflection angle:

$$\theta_{sph}(y,z) = \frac{M}{2n_{cr}} \int_{-d}^{D} \frac{\partial n_e}{\partial \rho} dx. \tag{12}$$

Looking at the Gaussian distribution case but in 3 dimensions, we arrive at

$$\theta_{sph,G}(y,z) = \rho A_{sph} \exp\left(B_{sph}\rho^2\right) \, , \tag{13}$$

where

$$A_{sph} = \gamma \frac{M\sqrt{\pi}n_0}{2n_{cr}} [\text{erf}(\gamma D) + \text{erf}(\gamma d)]$$
$$B_{sph} = -\gamma^2$$

Similarly, with a parabolic density profile in 3 dimensions, we arrive at

$$\theta_{sph,P}(y,z) = -\frac{n_0}{n_{cr}} \frac{M\rho}{r_f} \sqrt{2 - \left(\frac{\rho}{r_f}\right)^2}. \tag{14}$$

2.3 Discretized Solution

Equations 7, 10, 13, and 14 arrive at a solution by approximating the electron distribution with a function. It is important to also evaluate Eq. 1 with a discretized solution that can be solved and inverted directly from data. This method also lends itself to eventual 3-D reconstruction given 2 or more probe beams. We begin by differentiating Eq. 1 to get

$$\Delta\theta = \frac{1}{2n_{cr}}\nabla n_e \cdot \Delta\mathbf{x}, \tag{15}$$

Where $\Delta\mathbf{x}$ is a small movement in the direction of the probe laser propagation. Upon summation along the entire propagation direction from x_0 to x_n, we have

$$\theta = \sum_{x_0 \to x_n} \Delta\theta = \frac{M}{2n_{cr}}\sum_{i=1}^{n}\nabla n_e \cdot (x_i - x_{i-1}). \tag{16}$$

As an example, if we assume cylindrical geometry in Eq. 3 and inserted into Eq. 16, we arrive at

$$\theta_{cyl} = \frac{M}{2n_{cr}}\sum_{i=1}^{n}\frac{\partial n_e}{\partial y}(x_i - x_{i-1}) \tag{17}$$

with the understanding that $x_0 = -d$ and $x_n = D$. This yields 2 results,

$$\theta_{cyl,G} = \alpha M y \frac{n_0}{n_{cr}}\exp(\alpha y^2)\sum_{i=1}^{n}\exp(\alpha x_i^2)(x_i - x_{i-1}), \tag{18}$$

$$\theta_{cyl,P} = -\frac{Mn_0}{2n_{cr}r_f^2}y\sum_{i=1}^{n}(x_i - x_{i-1}), \tag{19}$$

depending on Gaussian and parabolic profile, respectively.

2.4 Phase Sensitivity to Electron Density

An important consideration that stems from Eqs. 7, 10, 13, and 14 is the maximum phase change the probe beam will experience across the extent of the plasma. In the cylindrical geometry case, by solving for $\partial\theta/\partial y = 0$, we arrive at

$$\theta_{cyl,G,max} = \pm\frac{A_{cyl}}{\gamma\sqrt{2}}\exp\left(-\frac{1}{2}\right) \tag{20}$$

$$\theta_{cyl,P,max} = \pm\frac{Mn_0}{n_{cr}} \tag{21}$$

for Gaussian and parabolic profiles, respectively. Similarly for spherical geometry and solving for $\partial\theta/\partial\rho = 0$,

$$\theta_{sph,G,max} = \pm\frac{A_{sph}}{\gamma\sqrt{2}}\exp\left(-\frac{1}{2}\right) \tag{22}$$

$$\theta_{sph,P,max} = \pm \frac{Mn_0}{n_{cr}} \qquad (23)$$

for Gaussian and parabolic profiles, respectively. The maximum phase change will help us to determine the sensitivity of an optical system given the probe wavelength, layout of the optics, extent of the plasma, and sensitivity of the Shack-Hartmann sensor.

3. Electron Densitometer Description

The Shack-Hartmann method offers a significant increase in resolution of phase changes, θ, in the laser probe beam. Because of the advanced algorithms used in proprietary software, small phase changes can be translated into perturbations smaller than the probe wavelength. A diagram of SHED is shown in Fig. 3b with the critical component being the Shack-Hartmann wavefront sensor (WFS). In this case, phasefront and wavefront can be used interchangeably. The selected WFS, as seen in Fig. 3c, is Imagine Optics's HASO3-128 GE featuring a 128×128 lenslet array mounted on a 12-bit CCD camera. The WFS has a $14.6\text{-} \times 14.6\text{-mm}^2$ aperture and is calibrated for a probe wavelength between 630 and 900 nm. The probe samples a cross section of approximately 2×2 mm^2, resulting in a magnification factor $M \approx 7$. The minimum sensitivity of the WFS is 1 μrad at 800 nm which, via Eq. 21, would equate to an electron density of $n_0 = 2.5 \times 10^{14}$ cm^{-3} in the parabolic case with cylindrical geometry. This can be considered a good approximation of the minimum recordable electron density for this SHED setup.
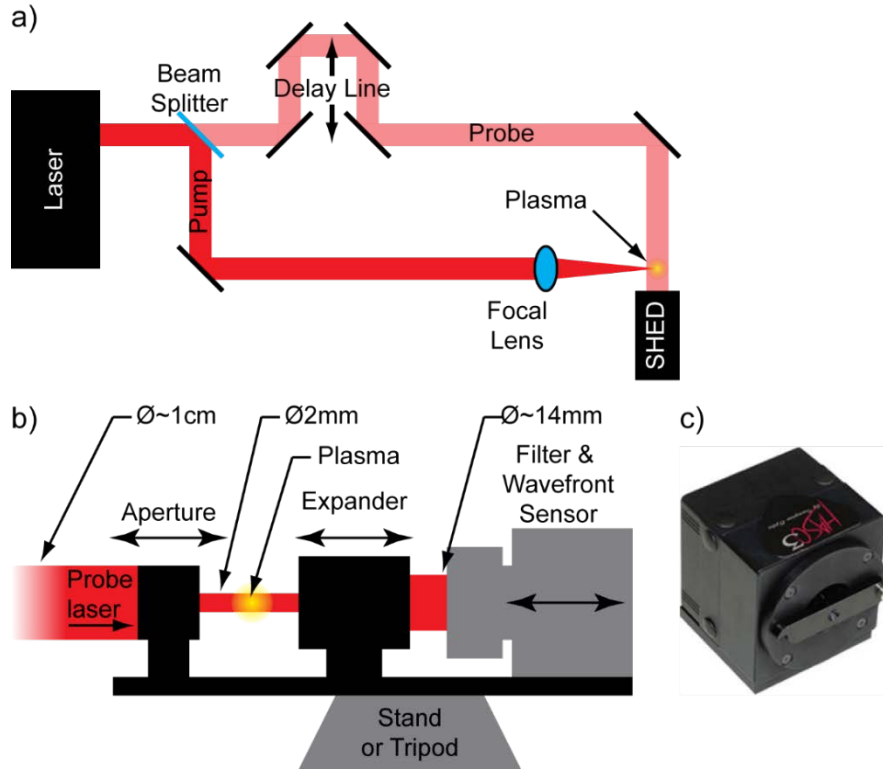
Fig. 3 Experimental components including a) the general optical setup with pump and probe beam path including a delay line, b) diagram of the Shack-Hartmann Electron Densitometer, and c) the HASO3 128 GE wavefront sensor

4. Experimental Setup

The electron densitometer was first tested with the US Army Research Laboratory's USPL located at Aberdeen Proving Ground (APG), Maryland. The laser system is the Coherent Hidra-25 that uses Titanium:Sapphire (Ti:Sapph) gain medium and chirped pulse amplification technologies. The system produces up to 20 mJ in 100 fs (peak power of up to 200 GW) at a repetition rate of up to 10 Hz at a wavelength of 800 nm. As shown schematically in Fig. 3a, the laser pulse passes through a beam splitter allowing for approximately 2% of the energy to be sent into the probe beam path and the rest (pump beam) used to generate the plasma in air. The probe beam is filtered with neutral density glass to prevent damage to SHED.

The plasma is created by focusing the pump beam either through geometric focusing, nonlinear self-focusing, or a combination of the 2. Higher-density plasmas are typically created with shorter focal length lens; higher-density plasmas are easier to diagnose in this case. Therefore, the experimental verification of SHED began with a 10-cm focal length lens and gradually worked to a longer focal distance. The probe beam is situated to cross near the focal point of the pump beam and overlap in time. With these shorter focal lengths, nonlinear self-focusing is

small compared to the geometric focus. This holds true until about 0.5-m focal length distances at which point we approach the criteria necessary for filamentation. In filaments, the energy is essentially stretched over a longer distance resulting in a lower electron density.

5. Results

Images captured on the WFS were translated into phasefront maps via Imagine Optic's Haso 3 software. The algorithms incorporated into the software are proprietary; however, the data were analyzed in a zonal fashion rather than a modal fashion given the lack of any anticipated radial symmetry in the probe direction. Tip and tilt are automatically corrected, and each acquisition is compared against a control image without a plasma. As shown in Fig. 4a, the probe beam intensity is greatly distorted, primarily from laser fluctuations and air turbulence. However, the Haso 3 software is able to retrieve a distinct signature (Fig. 4b) resulting from the laser-produced plasma in a single laser pulse. Despite the relative insensitivity to intensity variations in the probe beam, variations arising from the distortion of the phasefront from turbulence can have a significant effect. As seen in Fig. 5a, these variations are on the order of phasefront change resulting from the plasma as we moved to longer focal lenses and hence weaker plasmas. While the sensitivity of SHED is expected to be as low as 1 µrad, the effects of turbulence in the lab reduce this to the order of 100 s of milliradians. This result is emphasized further with a focal lens of 50 cm as seen in Fig. 6. This results in minimum recordable n_0 on the order of 10^{19} cm^{-3} as compared to the calculations represented in Fig. 5b. Also, the dip in the center of the phase change seen in Fig. 5b is not recorded in any of the phasefronts, likely due to a lack of fine resolution and variations from a radially symmetric plasma column.
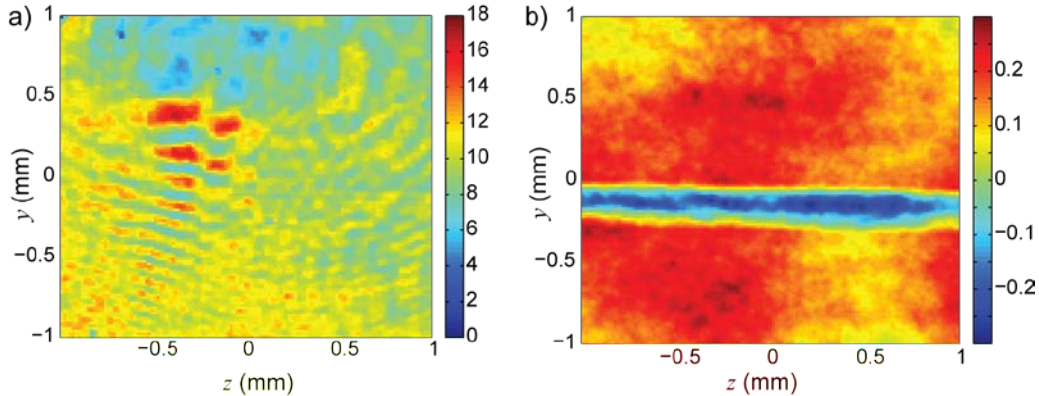
Fig. 4   Data gathered from probing of plasma created with f = 10 cm and E = 2 mJ: a) raw image with color scale in arbitrary units; b) HASO 3–generated phasefront map with color scale in radians
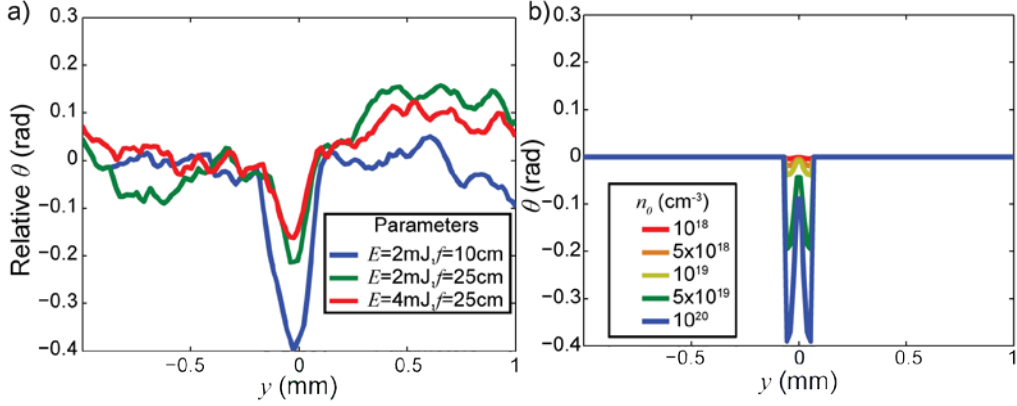
Fig. 5 **a) Cross section of phasefront map with the $E = 2$ mJ, $f = 10$-cm data corresponding to Fig. 4b. b) Phase change calculated from Eq. 10 based on varying electron densities and including a magnification factor, $M = 7$.**
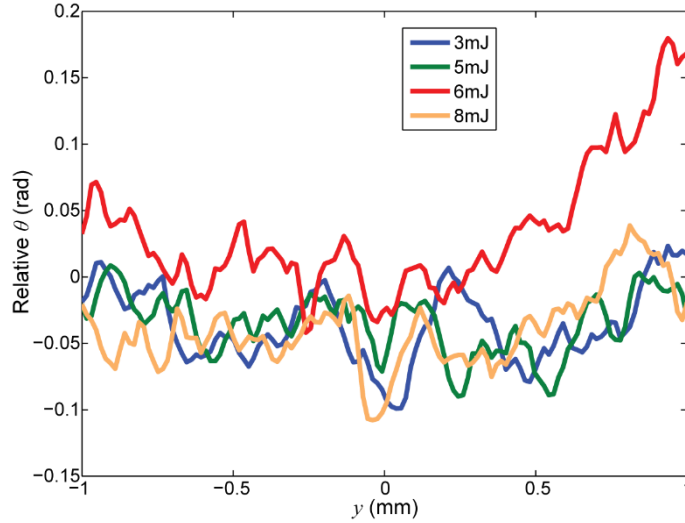
Fig. 6 **Cross section of phasefront map for $f = 50$ cm at varying energies**

In addition, by using a delay line in the path of the probe beam, one can image the evolution of the plasma. The advantage of using an ultrashort probe beam is to essentially freeze physical phenomenon. This can be seen in Fig. 7 where the front of the laser pulse is just starting to ionize air with full ionization across the SHED field of view within approximately 1.33 ps. With a 100-fs laser pulse, the spatial extent would only be approximately 30 µm, which would simultaneously cover about 2 lenslets at this magnification. As the plasma dynamics unfold long after the laser pulse has left, we see a gradual enlargement of the area of phasefront disturbance as the plasma dissipates and free electrons begin to recombine with ions. These dynamics happen well before any acoustic propagation of energy in the form of a shockwave as reported by Milchberg et al.[21]

11
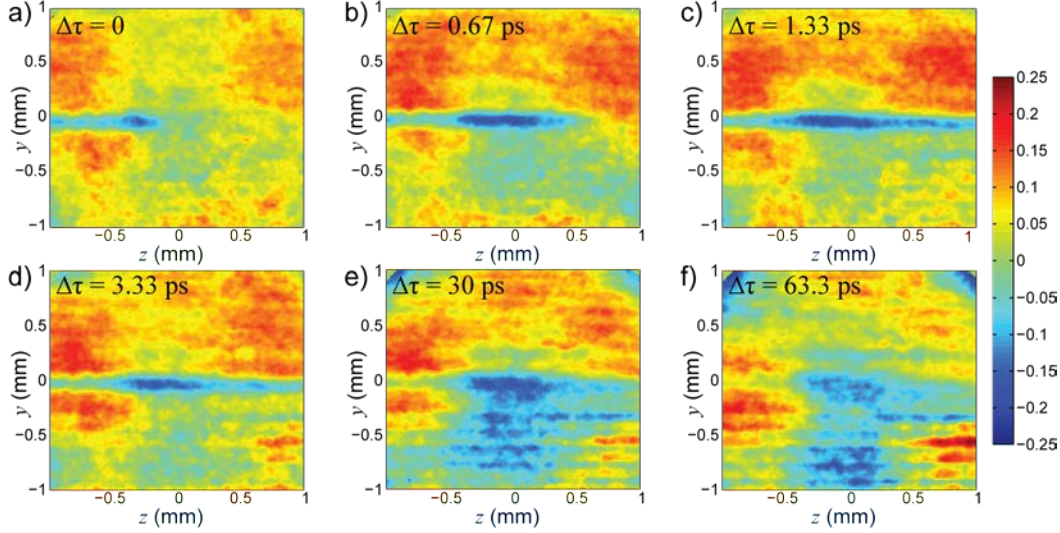
Fig. 7   Temporal scan of phasefront from E = 4.2 mJ, f = 25 cm where a) is an arbitrary t = 0, and relative delay shown in b–f.

6.   Future Work

Improvements planned in future work include turbulence mitigation and working toward a full 3-D reconstruction. As the data presented have demonstrated, effects from air turbulence and laser fluctuations can easily overwhelm the signal created by the plasma at longer focal lengths. While laser fluctuations can be handled with modifications and maintenance of the USPL, air turbulence remains a significant factor when probing over long propagation distances. The primary mitigation for this will be to enclose the probe beam as much as practicable. Certain areas such as the delay line present complications, but large enclosures can be helpful. Another tactic is to use higher-repetition-rate lasers with shorter pulse durations.[22] We plan to use the new USPL at APG (Coherent Astrella) that generates 30-fs pulses at a 1-kHz repetition rate at an 800-nm wavelength.

A further addition would be to split the probe beam into 2 orthogonal components crossing through the filament as shown in Fig. 8. By using tomographic mathematical techniques, researchers could produce a 3-D reconstruction of the filament plasma density with time resolution on the same scale as the initial laser pulse itself. A full picture can be derived by passing the probe beam through a spatial delay stage arriving at 4-D reconstruction of the evolution of the free electron density in a filament. This is accomplished by splitting the current probe beam into 2 components and passing one arm through a beta barium borate crystal that frequency doubles the wavelength to 400 nm. This reduces the potential for interference between all 3 beams and reduces the need for perfect orthogonality.

This also requires the WFS to be specially calibrated for that wavelength, which is an available option on the HASO 3.
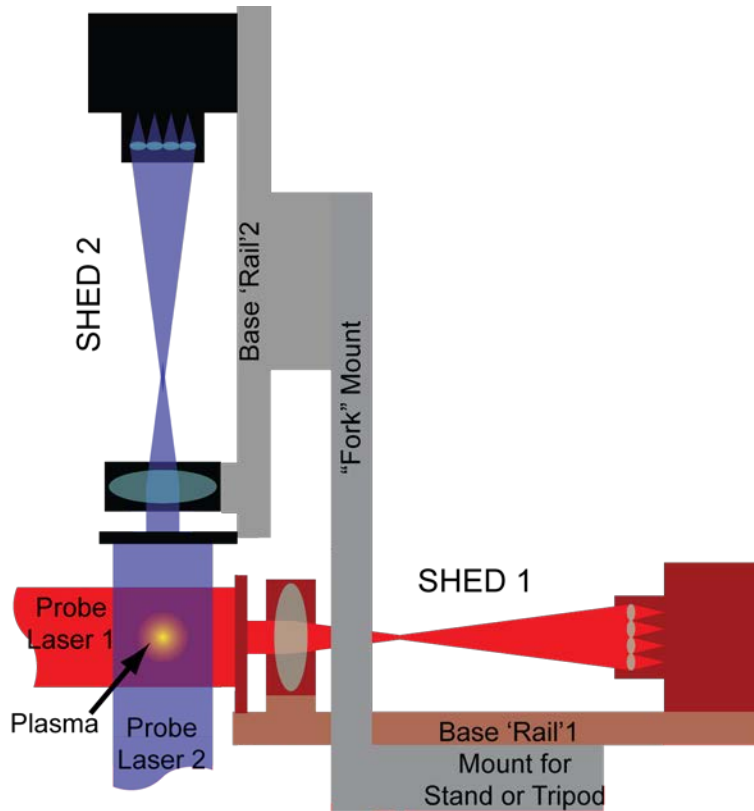
Fig. 8   A 2-axis SHED system for 3-D reconstruction of electron density profile; probe laser 2 is frequency doubled

7.   Conclusion

SHED offers a unique method to diagnose free electron density with at least 2-D resolution in a single shot. The precision afforded by using the Shack-Hartmann technique will allow for much finer density resolution than standard interferometry at these probe wavelengths. By using a portion of the same laser pulse to probe the plasma, ultrashort time resolutions are possible, detailing the evolution of free electrons during and after ionization. SHED has also been shown to be resilient to variations in the intensity of the probe laser beam; however, it is subject to phase variations created by the laser and air turbulence. Further refinement of SHED will lead to new understanding of the complex dynamics of USPL-created plasmas.

8. References

1. Couairon A, Mysyrowicz A. Femtosecond filamentation in transparent media. Phys Rep. 2007;441:47–189.

2. Bergé L, Skupin S, Nuter R, Kasparian J, Wolf J-P. Ultrashort filaments of light in weakly ionized, optically transparent media. Rep Prog Phys. 2007;70:1633–1713.

3. Kandidov VP, Shlenov SA, Kosareva OG. Filamentation of high-power femtosecond laser radiation. Quantum Electon. 2009;39(3):205–228.

4. Musin RR, Shneider MN, Zheltikov AM, Miles RB. Guiding radar signals by arrays of laser-induced filaments: finite-difference analysis. Appl Optics. 2007;46(23):5593–5597.

5. Dormidonov AE, Valuev VV, Dmitriev VL. Shlenov SA, Kandidov VP. Laser filament induced microwave waveguide in air. Proc of SPIE 2007;6733: 67332S.

6. Châteauneuf M, Payeur S, Dubois J, Kieffer J-C. Microwave guiding in air by a cylindrical filament array waveguide. Appl Phys Lett. 2008;92(9):091104.

7. Alshershby M, Hao Z, Lin J. Analysis of microwave leaky modes propagating through laser plasma filaments column waveguide. Phys Plasmas. 2012;19(12):123504.

8. Alshershby M, Ren Y, Qin J, Hao Z, Lin J. Diagnosis of femtosecond plasma filament by channeling microwaves along the filament. Appl Phys Lett. 2013;102(20);204101.

9. Ren Y, Alshershby M, Qin J, Hao Z, Lin J. Microwave guiding in air along single femtosecond laser filament. J Appl Phys. 2013;113(9):094904.

10. Guo K, Lin J, Hao Z, Gao X, Zhao Z, Sun C, Li B. Triggering and guiding high-voltage discharge in air by single and multiple femtosecond filaments. Opt Lett. 2012;37(2):259–261.

11. Henriksson M, Daigle J-F, Théberge F, Châteauneuf M, Dubois J. Laser guiding of Tesla coil high voltage discharges. Opt Express. 2012;20(12);12721–12728.

12. Leonov SB, Firsov AA, Shurupov MA, Michael JB, Shneider MN, Miles RB, Popov NA. Femtosecond laser guiding of a high-voltage discharge and the restoration of dielectric strength in air and nitrogen. Phys Plasmas. 2012;19(12):123502.

13. Bodrov S, Bukin V, Tsarev M, Murzanev A, Garnov S, Aleksandrov N, Stepanov A. Plasma filament investigation by transverse optical interferometry and terahertz scattering. Opt Express. 2011;19(7):6829–6835.

14. Chen Y-H, Varma S, Antonsen T M, Milchberg H M. Direct measurement of the electron density of extended femtosecond laser pulse-induced filaments. Phys Rev Lett. 2010;105(21):215005.

15. Wang T-J, Yu J, Wei Y, Li R, Xu Z, Chin S L. Longitudinally resolved measurement of plasma density along femtosecond laser filament via terahertz spectroscopy. Appl Phys Lett. 2014; 105 (5): 051101.

16. Rodriguez G, Valenzuela A R, Yellampalle B, Schmitt M J, Kim K-Y. In-line holographic imaging and electron density extraction of ultrafast ionized air filaments. J Opt Soc Am B. 2008;25(12):1988–1997.

17. Théberge F, Liu W, Simard P Tr, Becker A, Chin S L. Plasma density inside a femtosecond laser filament in air: Strong dependence on external focusing. Phys Rev E. 2006;74(3):036406.

18. Daigle J-F, Kosareva O, Panov N, Bégin M, Lessard F, Marceau C, Kamali Y, Roy G, Kandidov VP, Shin SL. A simple method to significantly increase filaments' length and ionization density. Appl Phys B. 2009;94:249–257.

19. Platt BC, Shack R. History and principles of Shack-Hartmann wavefront sensing. J. Refr Surg. 2001;17:S573-S577.

20. Baker K L, Brase J, Kartz M, Olivier SS, Sawvel B, Tucker J. The use of a Shack–Hartmann wave front sensor for electron density characterization of high density plasmas. Rev Sci Instr. 2002;73(11):3784–3788.

21. Milchberg HM, Chen Y-H, Cheng Y-H, Jhajj N, Palastro JP, Rosenthal EW, Varma S, Wahlstrand J K, Zahedpour S. The extreme nonlinear optics of gases and femtosecond optical filamentation. Phys Plasmas. 2014;21(10):100901.

22. Jhajj N, Cheng Y-H, Wahlstrand J K, Milchberg H M. Optical beam dynamics in a gas repetitively heated by femtosecond filaments. Opt Express. 2013;21(23):28980–28986.

List of Symbols, Abbreviations, and Acronyms

2-/3-/4-D	2-/3-/4-dimensional
APG	Aberdeen Proving Ground
CCD	charge-coupled device
SHED	Shack-Hartmann Electron Densitometer
USPL	ultrashort pulse laser
WFS	wavefront sensor

1 (PDF)	DEFENSE TECHNICAL INFORMATION CTR DTIC OCA
2 (PDF)	DIRECTOR US ARMY RESEARCH LAB RDRL CIO L IMAL HRA MAIL & RECORDS MGMT
1 (PDF)	GOVT PRINTG OFC A MALHOTRA

12
(10 PDF,
2 HC)
	DIR USARL
	RDRL WML B
	  F DELUCIA
	  J GOTTFRIED
	RDRL WML C
	  C MUNSON
	RDRL WMP A
	  S BILYK
	  J FLENIKEN
	  T KOTTKE
	  A SCHWEINSBERG
	  W UHLIG
	  A VALENZUELA (2 HC)
	  L VANDERHOEF
	  C WOLFE

INTENTIONALLY LEFT BLANK.